Euro. Jnl of Applied Mathematics (2008), *vol.* 19, *pp.* 41–60.
doi:10.1017/S0956792507007279 Printed in the United Kingdom

Invasion around a horizontal wellbore

V. V. SHELUKHIN

Lavrentyev Institute of Hydrodynamics, Lavrentyev pr. 15, Novosibirsk 630090, Russia
email: shelukhin@hydro.nsc.ru

(*Received 27 March 2007; revised 3 December 2007*)

A mathematical model is developed for mud cake growth and fluid invasion around a horizontal wellbore during drilling. The non-axisymmetry of the invasion front is addressed for the case of water based drilling mud and isotropic rock formation. It is shown that the invasion profile may lose convexity due to gravitation even though the filtrate density is the same as that of the pore fluid in the rock.

1 Introduction

It is well known that formation damage caused by drilling-fluid invasion should be taken into account, both for correct interpretation of logging data and for prediction of well performance for natural clean-up when the well is subject to a pressure drawdown [3]. A series of laboratory experiments was conducted to study the mud induced formation damage around a horizontal wellbore [1], [10], [14].

Motivated by these experiments, we consider invasion of filtrate from a horizontal wellbore into pores of surrounding rock. The pressure within the wellbore is higher than that within the pores of the formation. In addition, the density of the drilling mud is different from that within the pores. This leads to a boundary condition on the pressure within the wellbore that depends on the vertical position x_2, thereby breaking the axisymmetry. Fluid leaves the wellbore and deposits particles (typically clay particles or barite weighting agent particles within the mud suspension) on the surface of the rock. Due to this deposition, a mud cake grows with time. To describe the growth, we derive a rather general transport equation for mud cake thickness considering the mud as a two-phase fluid. The mud cake face is treated as a shock surface propagating through the mud, with the solid-phase parameters (velocity, density and concentration) undergoing jumps in agreement with the solid mass conservation law; the solid phase stiffens behind the shock front and contributes to the growing rigid mud cake. It is the Rankine-Hugoniot jump condition that gives rise to the mud cake transport equation. Then we find a good approximation of the mud cake equation for the case when mud circulation in the wellbore is not strong and concentration of solids in mud is small. Relating mud cake growth with fluid flux into the formation, this simpler mud cake equation enables us to evaluate the formation damage by means of analytical tools only.

Measurements with water-saturated sands [10] have revealed loss of convexity of the brine invasion front with time. This effect is captured by our model as can be seen from the calculations in Section 10; it is an interesting feature of the invasion profile that it

has a cusp sometimes forming on the upper or lower part of the profile depending on the mud fluid density–pore fluid density ratio (see Figure 4).

In some research, the growing mud cake is modelled as if it were an extension to the porous formation; such an approach requires a remeshing for the next time step while developing a finite element code [4]. Our mathematical model takes into account the mud cake hydraulic resistance by means of a boundary-value condition for pressure in a fixed formation domain. In comparison with the results of [3], the novelty is that this condition depends strongly both on the mud cake thickness and the difference in density between the mud and a formation fluid. To determine the pressure drop across the mud cake we use an asymptotic argument, with the mud cake thickness being a small parameter.

Mud cake build-up for vertical wellbores has been the subject of a number of other investigations [8], [13] but no advanced electro-kinetic theory has been developed yet to identify the mud cake porosity and permeability, so it is commonly assumed that these two basic parameters are given by specific measurements.

As mentioned in the above laboratory experiments, we do not take into account the mud cake disturbance by motion of the drill string, which will generally rest on the lower surface of a horizontal well.

The paper is organised as follows. In Sections 2 and 3 we discuss how the mud cake interferes between the wellbore and the rock formation, and we derive a free-boundary problem for the mud cake growth. In Section 4, under the hypothesis of thin mud cake, we simplify by passing to a fixed-domain problem which still allows for both the invasion of drilling mud into the formation and the accumulation of solid particles on the inside of the wellbore. Section 5 is devoted to an asymptotic analysis of the reservoir pressure equations. Invasion-front equations are derived in Section 6. In final sections we analyse the governing equations analytically and numerically.

2 Governing equations for pressure

As soon as the drilling bit comes in contact with the reservoir, there is a rapid fluid invasion (spurt loss) because there is no filter cake to prevent fluid solid particles from entering into the pay zone. During this period, there is a progressive deposition of these particles which creates an internal filter cake.

We consider here the process when this internal filter cake is well established, most of the solid particles are retained outside the formation, generally creating a thin external mud cake, which mainly controls the rate of filtration invasion.

The mathematical model proposed below describes the situation where the invading and formation fluids have identical viscosities and the mud density ρ_m differs from the density of the formation fluid ρ_f^r only slightly. In this case, the fluid invading the formation loses clay particles on the wellbore wall, overcomes the additional hydraulic resistance of the filtrate cake and, when entering the formation, has the same density as the formation fluid [11].

We study two-dimensional flows in a vertical (x_1, x_2)-plane perpendicular to the horizontal wellbore. The flow scheme is depicted in Figure 1. The cross-section of the wellbore is a circle of radius R_0 with centre at the coordinate origin. The x_2-axis is vertical and the x_1-axis is directed to the right parallel to the plane tangent to the ground. We consider

https://doi.org/10.1017/S0956792507007279 Published online by Cambridge University Press

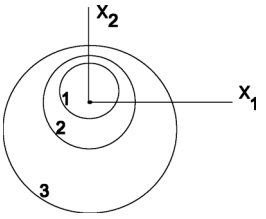

FIGURE 1. 1-line is the mud cake face, 2-line is the wellbore wall, 3-line is the invasion front.

the flow in the region separated from the centre of the wellbore by a distance not larger than R_∞; therefore cylindrical variables (r, θ) are used below and the angle θ is measured anti-clockwise from the x_1-axis.

Incompressible flows in the formation are governed by the Darcy law

$$\mathbf{q} = -\lambda_r \nabla\left(p + \rho_f^r g x_2\right), \quad \operatorname{div} \mathbf{q} = 0, \quad r_c \equiv R_0 < r < R_\infty. \tag{2.1}$$

Here, $\mathbf{q}$ is the Darcy velocity vector, p is the pressure, h is the discharge or potential, λ_r is the mobility of the formation fluid, g is the gravitational acceleration constant. We recall that $\lambda_r = k_r/\mu_r$, where k_r is the formation permeability, μ_r is the viscosity of the reservoir fluid.

Equations (2.1) are valid in the annulus $R_0 < r < R_\infty$. Away from the wellbore, at $r = R_\infty$, the pressure is distributed according to the hydrostatic law and hence the following boundary condition is satisfied:

$$r = R_\infty : \quad h \equiv p + \rho_f^r g x_2 = p_\infty = \text{const}. \tag{2.2}$$

As for the flows in the mud cake, governing equations are the same:

$$\mathbf{q} = -\lambda_c \nabla\left(p + \rho_f^r g x_2\right), \quad \operatorname{div} \mathbf{q} = 0, \quad r_c \equiv R_0 - \sigma(\theta) < r < R_0. \tag{2.3}$$

Here, $\sigma(\theta)$ is the mud cake thickness, $\lambda_c = k_c/\mu_r$, with k_c being the mud cake formation permeability. It is assumed that the formation fluid density and the mud filtrate density coincide and take a value ρ_f^r while the drilling mud density ρ_m may be different.

Given a function $f(r)$, we introduce its jump at a point of discontinuity R_0:

$$f|_{R_0 \pm 0} = f^\pm = \lim_{\delta \to 0} f(R_0 \pm \delta), \quad [f] = f^+ - f^-.$$

In what follows, $\partial_x = \partial/\partial x$ denotes the partial derivative in a variable x.

Pressure, density and mass flux are continuous across the surface $r = R_0$. Hence, h obeys the boundary conditions $[h] = 0$ and $[\lambda \partial_r h] = 0$, i.e.

$$h|_{r=R_0-0} = h|_{r=R_0+0}, \quad \lambda_c \partial_r h|_{r=R_0-0} = \lambda_r \partial_r h|_{r=R_0+0}. \tag{2.4}$$

Let us calculate the jump of h across the surface $r = r_c$, assuming that the mud circulation is governed by the Euler equations for irrotational incompressible flows. In this case, the Bernoulli integral holds, i.e.

$$\rho_m \mathbf{v}^2/2 + p + \rho_m g x_2 = const.$$

https://doi.org/10.1017/S0956792507007279 Published online by Cambridge University Press

Therefore, the potential $p + \rho_m g x_2$ is constant along the mud cake face as long as $|\mathbf{v}|$ is constant. Thus, we require that

$$h|_{r=r_c-0} \equiv (p + \rho_m g x_2)|_{r=r_c-0} = p_w = const.$$

The constant p_w is identified as the value of the potential h in the wellbore mud close to the mud cake face. Particularly, the above equality holds if the drilling mud pressure at the mud cake surface is distributed according to the hydrostatic law.

Pressure is continuous across the free boundary, so we write $[p] = 0$ at $r = r_c$, i.e.

$$h|_{r=r_c+0} = p_w + [h] = p_w + [\rho] g \sin\theta (R_0 - \sigma),$$

where $[\rho] = \rho_f^r - \rho_m$.

In the next section, we derive an evolution equation for the unknown mud cake thickness function $\sigma(t, \theta)$.

3 Mud cake dynamics: free-boundary equation

Here we discuss the question of deposition of solid particles on the inside of the wellbore for general three-dimensional mud flows. Our approach is based on the mass conservation law for the solid phase of the mud fluid [6]:

$$\frac{\partial(\rho_s \varphi_s)}{\partial t} + \operatorname{div}(\rho_s \varphi_s \mathbf{v}_s) = 0. \tag{3.1}$$

Here, ρ_s is the density of solid particles in the mud, φ_s is the volume concentration of solids in the mud and $\mathbf{v}_s$ is the solid phase velocity. We recall that $\varphi_s + \varphi_f = 1$, where φ_f is the volume concentration of the mud fluid phase. Equation (3.1) is considered in the three-dimensional domain

$$-\infty < x_3 < +\infty, \quad R_1 < r < R_0,$$

where R_1 stands for the drill string radius.

We assume that:

(i) equation (3.1) holds in the distributional sense in the entire domain $R_1 < r < R_0$;

(ii) equation (3.1) holds in the classical sense both in the shear flow domain $R_1 < r < r_c(t, \theta, x_3)$ and in the mud cake domain $r_c(t, \theta, x_3) < r < R_0$, with the functions ρ_s φ_s and $\mathbf{v}_s$ being continuous everywhere except the shock surface:

$$r = r_c(t, \theta, x_3), \tag{3.2}$$

separating the rigid zone $r_c(t, \theta, x_3) < r < R_0$ from the flowing solid phase $R_1 < r < r_c(t, \theta, x_3)$. In the mud cake zone, we have

$$\rho_s = \rho_c, \quad \varphi_s = 1 - \Phi_c, \quad \mathbf{v}_s = 0,$$

where ρ_c is the skeleton density and Φ_c is the mud cake porosity.

https://doi.org/10.1017/S0956792507007279 Published online by Cambridge University Press

Let us write equation (3.1) for flows in the cylindrical variables:

$$\frac{\partial(r\rho_s\varphi_s)}{\partial t}+\frac{\partial(r\rho_s\varphi_s u_s)}{\partial r}+\frac{\partial(r\rho_s\varphi_s w_s)}{\partial z}+\frac{\partial(\rho_s\varphi_s v_s)}{\partial\theta}=0, \tag{3.3}$$

where u_s is the radial velocity component, v_s is the circumferential velocity component and w_s is the axial velocity component.

The calculation of jumps across the free-boundary (3.2) can be performed as in the theory of shocks in conservation laws [12]. Let $[f]$ stand for the jump of a function $f(t,r,\theta,x_3)$ across the surface (3.2). Then the usual Rankine-Hugoniot condition for (3.3) leads to the jump condition

$$[r\rho_s\varphi_s]\frac{\partial r_c}{\partial t}-[r\rho_s\varphi_s u_s]+[r\rho_s\varphi_s w_s]\frac{\partial r_c}{\partial x_3}+[\rho_s\varphi_s v_s]\frac{\partial r_c}{\partial\theta}=0.$$

We write this as a general transport equation for the mud cake thickness σ:

$$\frac{\partial\sigma}{\partial t}+\frac{[\rho_s\varphi_s u_s]}{[\rho_s\varphi_s]}=-\frac{[\rho_s\varphi_s w_s]}{[\rho_s\varphi_s]}\cdot\frac{\partial\sigma}{\partial x_3}-\frac{[\rho_s\varphi_s v_s]}{[\rho_s\varphi_s](R_0-\sigma)}\cdot\frac{\partial\sigma}{\partial\theta}. \tag{3.4}$$

We recall that $\mathbf{v}_s|_{r_c+0}=0$, so

$$[\rho_s\varphi_s u_s]=-\rho_s^-\varphi_s^- u_s^-,\ [\rho_s\varphi_s w_s]=-\rho_s^-\varphi_s^- w_s^-,\ [\rho_s\varphi_s v_s]=-\rho_s^-\varphi_s^- v_s^-. \tag{3.5}$$

Equation (3.4) holds for any three-dimensional mud flow in the wellbore. Let us simplify it. First, in two-dimensional case $\partial\sigma/\partial_{x_3}=0$. Second, if the circulation of the viscous mud is not strong and concentration of solids in mud is small, the last term on the right-hand side of (3.4) is negligible. Under these assumptions, equation (3.4) becomes

$$\partial_t\sigma+[\rho_s\varphi_s u_s]/[\rho_s\varphi_s]=0. \tag{3.6}$$

Let Φ_c and ρ_c stand for the mud cake porosity and mud cake skeleton density. Then

$$[\rho_s\varphi_s]=(\rho_s\varphi_s)|_{r=r_c+0}-(\rho_s\varphi_s)|_{r=r_c-0}=\rho_c(1-\Phi_c)-\rho_s^-\varphi_s^-,$$

where ρ_s^- is the density of the mud solids and φ_s^- is the volume concentration of solid particles in the mud.

One can assume that

$$u_s^+=0,\quad u_s^-=\alpha u_f^-, \tag{3.7}$$

where α is a relative velocity factor and u_f is the radial component of the velocity vector of the mud fluid phase. In Section 7, we comment on the evaluation of the parameter α.

The fluid mass conservation law at the mud cake face reads

$$\rho_f^w\varphi_f^- u_{f,n}^-=\rho_f^r\Phi_c u_{f,n}^+, \tag{3.8}$$

where ρ_f^w is the density of the fluid phase in the mud and $u_{f,n}$ is the projection of the fluid velocity vector onto the unit normal $\mathbf{n}$ to the mud cake face curve $r+\sigma(t,\theta)-R_0=0$;

https://doi.org/10.1017/S0956792507007279 Published online by Cambridge University Press

the vector $\mathbf{n}$ is directed into the mud cake. We find that

$$\mathbf{n} = (\cos\theta - r_c^{-1}\partial_\theta\sigma \sin\theta,\ \sin\theta + r_c^{-1}\partial_\theta\sigma\cos\theta)/\sqrt{1+|\partial_\theta\sigma|^2/r_c^2}, \tag{3.9}$$

where $r_c = R_0 - \sigma$.

Let us find a relationship between the radial fluid velocity u_f and the normal fluid velocity $u_{f,n}$. By definition, $u_{f,n} = \mathbf{v}_f \cdot \mathbf{n}$. We have $\mathbf{v}_f = (u_f\cos\theta - v_f\sin\theta, u_f\sin\theta + v_f\cos\theta)$, so

$$\mathbf{v}_f \cdot \mathbf{n} = n_1(u_f\cos\theta - v_f\sin\theta) + n_2(u_f\sin\theta + v_f\cos\theta),$$

where v_f is the circumferential component of velocity vector of the mud fluid phase. The mud fluid angular circulation near the mud cake face is negligible, i.e. $v_f^- = 0$. Thus,

$$u_{f,n}^- = u_f^-/\sqrt{1+|\partial_\theta\sigma|^2/r_c^2}.$$

We calculate

$$\frac{\rho_s^-\varphi_s^- u_s^-}{[\rho_s\varphi_s]} = \frac{\alpha\rho_s^-\varphi_s^-\rho_f^r\Phi_c u_{f,n}^+}{[\rho_s\varphi_s]\rho_f^w\varphi_f^-}\sqrt{1+|\partial_\theta\sigma|^2/r_c^2}.$$

By the Darcy law,

$$\Phi_c u_{f,n}^+ = -\lambda_c\nabla h\cdot\mathbf{n}|_{r=r_c+0},$$

where h is the mud cake potential. Hence, equation (3.6) becomes

$$\partial_t\sigma = -A\sqrt{1+|\partial_\theta\sigma|^2/r_c^2}\,\nabla h\cdot\mathbf{n}|_{r=r_c+0}, \quad A = \frac{\alpha\rho_s^-\varphi_s^-\rho_f^r\lambda_c}{[\rho_s\varphi_s]\rho_f^w\varphi_f^-}. \tag{3.10}$$

Finally, the complete formulation of the free-boundary problem is now obtained by combining all the equations and the boundary conditions. We look for two functions $h(t,r,\theta)$ and $\sigma(t,\theta)$ such that

$$\begin{aligned} \operatorname{div}(\lambda\nabla h) = 0, \quad r_c \equiv R_0 - \sigma(t,\theta) < r < R_\infty,\\ h|_{r=R_\infty} = p_\infty, \quad [h]|_{r=R_0} = 0, \quad [\lambda\nabla h\cdot\mathbf{n}]|_{r=R_0} = 0,\\ h|_{r=r_c+0} = p_w + g(R_0-\sigma)(\rho_f^r - \rho_m)\sin\theta,\\ \partial_t\sigma = -A\sqrt{1+|\partial_\theta\sigma|^2/r_c^2}\,\nabla h\cdot\mathbf{n}|_{r=r_c+0}, \quad \sigma|_{t=0} = 0, \end{aligned} \tag{3.11}$$

where

$$\lambda(r) = (\lambda_r - \lambda_c)\frac{\operatorname{sign}(r-R_0)}{2} + \frac{\lambda_r+\lambda_c}{2},$$

and $\mathbf{n}$ at $r = r_c$ is given by (3.9).

We remark that one should apply the general equation (3.4) as far as mud circulation is strong. In that case, the right-hand side terms are 'removable terms' which are responsible for the mud cake stabilisation.

4 Non-dimensionalisation and approximate equations

The free-boundary problem formulated above is strongly degenerate since the two-dimensional mud cake domain is initially a one-dimensional line. The most natural

https://doi.org/10.1017/S0956792507007279 Published online by Cambridge University Press

way forward is to develop a suitable approximation procedure. To this end we need to characterize the problem in terms of the sizes of various parameters. These parameters are introduced by defining a set of non-dimensional variables

$$\hat{h} = h/p_\infty, \quad \eta = \sigma/\sigma_*, \quad \hat{p}_w = p_w/p_\infty, \quad s = t/\tau, \quad r_\infty = R_\infty/R_0, \quad \varepsilon = \sigma_*/R_0,$$

where σ_* is the typical mud cake thickness, ε is the relative mud cake thickness and τ is the characteristic time interval.

By the change of variables $(r, \theta) \to (\xi, \theta)$, where

$$\xi = \frac{r - R_0}{\sigma_* \eta(\theta)} + 1,$$

we map the ε-dependent mud cake domain $1 - \varepsilon\eta(\theta) < r/R_0 < 1$ onto a fixed domain

$$0 < \xi < 1, \quad -\pi < \theta < \pi,$$

which does not depend on ε. In this domain, the function $\hat{h}(\xi, \theta)$, which is 2π-periodic with respect to θ, solves the equation

$$\begin{aligned}\big(\varepsilon^2\eta^2(\xi - 1) + \varepsilon\eta + \varepsilon^2(1 - \xi)\big(\partial_\theta^2\eta - |\partial_\theta\eta|^2\big)\big)\partial_\xi\hat{h} + 2\varepsilon^2\partial_\theta\eta(1 - \xi)\partial_\theta\partial_\xi\hat{h} \\ + (\varepsilon^2\eta^2(\xi - 1)^2 + 2\varepsilon\eta(\xi - 1) + 1 + \varepsilon^2(\xi - 1)^2|\partial_\theta\eta|^2)\partial_\xi^2\hat{h} + \varepsilon^2\eta^2\partial_\theta^2\hat{h} = 0. \qquad (4.1)\end{aligned}$$

The transformation $(r, \theta) \to (\xi, \theta)$, $\xi = r/R_0$ maps the reservoir annulus $R_0 < r < R_\infty$ onto the domain

$$1 < \xi < r_\infty, \quad -\pi < \theta < \pi.$$

In this domain, the Laplace equation for $\hat{h}$ becomes

$$\xi\partial_\xi(\xi\partial_\xi\hat{h}) + \partial_\theta^2\hat{h} = 0 \quad \text{with} \quad \hat{h}|_{\xi = r_\infty} = 1 \quad \text{and} \quad \hat{h}(\xi, -\pi) = \hat{h}(\xi, \pi). \qquad (4.2)$$

The continuity conditions (2.4) at $r = R_0$ are now written as

$$[\hat{h}]|_{\xi=1} = 0, \quad \tilde{\lambda}\varepsilon\eta\partial_\xi\hat{h}|_{\xi=1+0} = \partial_\xi\hat{h}|_{\xi=1-0}, \quad \tilde{\lambda} \equiv \lambda_r/\lambda_c. \qquad (4.3)$$

The free-boundary reduces to the line $\xi = 0$ and the free-boundary conditions become

$$\hat{h}|_{\xi=0} = \hat{p}_w + \delta(1 - \varepsilon\eta)\sin\theta, \quad a\partial_s\eta = -\left(\frac{\partial_\xi\hat{h}}{\varepsilon^2\eta} + \frac{\partial_\theta\eta(\partial_\theta\hat{h} + \eta^{-1}\partial_\xi\hat{h}\partial_\theta\eta)}{(1 - \varepsilon\eta)^2}\right)\Bigg|_{\xi=0}, \qquad (4.4)$$

where

$$\delta = g\big(\rho_f^r - \rho_m\big)R_0/p_\infty, \quad a = \frac{R_0^2}{A\tau p_\infty} \qquad (4.5)$$

are dimensionless parameters.

https://doi.org/10.1017/S0956792507007279 Published online by Cambridge University Press

In applications, both ε and δ are small. When δ is not related to ε, it suggests that we seek a solution in the form of the asymptotic expansion

$$\hat{h} = h^{(0)}(s,r,\theta) + \varepsilon h^{1,0}(s,r,\theta) + \delta h^{0,1}(s,r,\theta) + \varepsilon\delta h^{1,1}(s,r,\theta) + \cdots,$$
$$\eta = \eta^{(0)}(s,r,\theta) + \varepsilon \eta^{1,0}(s,r,\theta) + \delta \eta^{0,1}(s,r,\theta) + \varepsilon\delta \eta^{1,1}(s,r,\theta) + \cdots.$$

But this approach does not work. Indeed, tedious calculations reveal the equation

$$a\eta^{(0)}\partial_s \eta^{(0)} = \eta^{1,0}(\hat{p}_w - 1)/\ln r_\infty.$$

It means that to determine the zero-order approximation term one should know first the first-order term. Similar irregular equations occur for higher-order terms. The reason is that the right-hand side of $(4.4)_2$ is not an analytic function of ε [9].

In order to make the problem more manageable, we argue as in the theory of surface waves of small amplitude [7]. We substitute the evaluation on the unknown free surface $\xi = 0$ by an evaluation on the known surface $\xi = 1$, even though the unknown mud cake thickness η still appears in the equations. We look for a mud cake potential $\hat{h}$ and thickness η given by the asymptotic series:

$$\hat{h} = \sum_0^\infty \varepsilon^k h^{(k)}(s,\xi,\theta,\delta), \quad \eta = \sum_0^\infty \varepsilon^k \eta^{(k)}(s,\xi,\theta,\delta). \tag{4.6}$$

Putting (4.6) in (4.1), $(4.3)_1$, and $(4.4)_1$ one can write each of these equalities in the form

$$\sum_0^\infty \varepsilon^k (\cdots)_k = 0.$$

To find all the coefficients $h^{(k)}(s,\xi,\theta,\delta)$, one should solve all the equations $(\cdots)_k = 0$. Particularly to find $h^{(0)}$ and $h^{(1)}$, one should solve the following boundary-value problems:

$$\partial_\xi^2 h^{(0)} = 0, \quad h^{(0)}|_{\xi=0} = \hat{p}_w + \delta\sin\theta \equiv \gamma_0, \quad h^{(0)}|_{\xi=1} = h_+^0,$$
$$\partial_\xi^2 h^{(1)} + \eta^{(0)}\partial_\xi h^{(0)} + 2\eta^{(0)}(\xi - 1)\partial_\xi^2 h^{(0)} = 0, \quad h^{(1)}|_{\xi=0} = -\delta\eta^{(0)}\sin\theta, \quad h^{(1)}|_{\xi=1} = h_+^1,$$

where

$$\hat{h}|_{\xi=1+0} = h_+^0 + \varepsilon h_+^1 + o(\varepsilon).$$

Solutions are given by the representation formulas

$$h^{(0)} = \hat{\gamma}\xi + \gamma_0, \quad \hat{\gamma} \equiv h_+^0 - \gamma_0,$$
$$h^{(1)} = -\xi^2\eta^{(0)}\hat{\gamma}/2 + \xi\left(h_+^1 + \eta^{(0)}\delta\sin\theta + \eta^{(0)}\hat{\gamma}/2\right) - \delta\eta^{(0)}\sin\theta.$$

The function $h^{(0)} + \varepsilon h^{(1)}$ could be taken as a first-order approximation of the mud cake potential $\hat{h}|_{0<\xi<1}$. Since

$$\varepsilon\eta = \varepsilon\eta^{(0)} + o(\varepsilon), \quad \hat{h}|_{\xi=1+0} - \left(h_+^0 + \varepsilon h_+^1\right) = o(\varepsilon),$$

https://doi.org/10.1017/S0956792507007279 Published online by Cambridge University Press

the function

$$\xi(\hat{h}|_{\xi=1+0}-\gamma_0)+\gamma_0-\xi^2\varepsilon\eta(\hat{h}|_{\xi=1+0}-\gamma_0)/2+\xi(\varepsilon\eta\delta\sin\theta+\varepsilon\eta(\hat{h}|_{\xi=1+0}-\gamma_0)/2)-\delta\varepsilon\eta\sin\theta \tag{4.7}$$

is a first-order approximation also. Then we make use of the function $\hat{h}|_{0<\xi<1}$ given by the representation formula (4.7) to calculate the right-hand sides of equalities $(4.3)_2$ and $(4.4)_2$. As a result, we obtain, denoting $\hat{\sigma}=\varepsilon\eta$, the following boundary conditions for the reservoir potential $\hat{h}|_{1<\xi<r_\infty}$ at $\xi=1$:

$$\tilde{\lambda}\hat{\sigma}\partial_\xi\hat{h}+(\hat{p}_w-\hat{h})(1-\hat{\sigma}/2)+\delta(1-3\hat{\sigma}/2)\sin\theta=0, \tag{4.8}$$

$$a\hat{\sigma}\partial_s\hat{\sigma}=(\hat{p}_w-\hat{h})(1+\hat{\sigma}/2)\left(1+\frac{|\partial_\theta\hat{\sigma}|^2}{(1-\hat{\sigma})^2}\right)-\frac{\delta\hat{\sigma}\partial_\theta\hat{\sigma}\cos\theta}{(1-\hat{\sigma})}$$
$$+\delta\sin\theta\left(1-\hat{\sigma}/2+(1+\hat{\sigma}/2)\frac{|\partial_\theta\hat{\sigma}|^2}{(1-\hat{\sigma})^2}\right),\quad \hat{\sigma}|_{s=0}=0. \tag{4.9}$$

Thus, under the hypothesis of thin mud cake we have derived a boundary-value problem in the fixed reservoir domain $1<\xi<r_\infty$ for the reservoir potential $\hat{h}$ and the mud cake thickness η. In what follows, this boundary-value problem, consisting of the equations and boundary conditions (4.2), (4.8) and (4.9), will underlie our analysis of the invasion front.

5 Mud cake growth and reservoir pressure development

We perform an asymptotic analysis of problem (4.2), (4.8) and (4.9), assuming that the parameter δ is small. We look for a solution in the form

$$\hat{h}=\sum_0^\infty\delta^k h_k,\quad \hat{\sigma}=\sum_0^\infty\delta^k\sigma_k. \tag{5.1}$$

Putting (5.1) into (4.2), (4.8) and (4.9), we find that h_0 and σ_0 solve the problem

$$\xi\partial_\xi(\xi\partial_\xi h_0)+\partial_\theta^2 h_0=0, \tag{5.2}$$

$$\xi=1:\quad \tilde{\lambda}\sigma_0\partial_\xi h_0+(\hat{p}_w-h_0)(1-\sigma_0/2)=0,\quad h_0|_{\xi=r_\infty}=1, \tag{5.3}$$

$$\xi=1:\quad a\sigma_0\partial_s\sigma_0=(\hat{p}_w-h_0)(1+\sigma_0/2)\left(1+\frac{|\partial_\theta\sigma_0|^2}{(1-\sigma_0)^2}\right). \tag{5.4}$$

Given functions h_0 and σ_0, one can find functions h_1 and σ_1 from the system

$$\xi\partial_\xi(\xi\partial_\xi h_1)+\partial_\theta^2 h_1=0,\quad h_1|_{\xi=r_\infty}=0, \tag{5.5}$$

$$\xi=1:\quad \tilde{\lambda}(\sigma_0\partial_\xi h_1+\sigma_1\partial_\xi h_0)=(\hat{p}_w-h_0)\sigma_1/2+\left(1-\sigma_0/2\right)h_1-(1-3\sigma_0/2)\sin\theta, \tag{5.6}$$

https://doi.org/10.1017/S0956792507007279 Published online by Cambridge University Press

$$\xi = 1: \quad a\sigma_0(1-\sigma_0)^2\partial_s\sigma_1 + a\partial_s\sigma_0(\sigma_1(1-\sigma_0)^2 - 2\sigma_0(1-\sigma_0)\sigma_1)$$
$$= 2(\hat{p}_w - h_0)(1+\sigma_0/2)(\partial_\theta\sigma_0\partial_\theta\sigma_1 - \sigma_1(1-\sigma_0)) - \sigma_0(1-\sigma_0)\partial_\theta\sigma_0\cos\theta$$
$$+((1-\sigma_0)^2 + |\partial_\theta\sigma_0|^2)\left(\frac{\sigma_1}{2}(\hat{p}_w - h_0) - h_1\left(1+\frac{\sigma_0}{2}\right)\right)$$
$$+((1-\sigma_0)^2(1-\sigma_0/2) + (1+\sigma_0/2)|\partial_\theta\sigma_0|^2)\sin\theta \tag{5.7}$$

The solution of problem (5.2)–(5.3) is given by the formula

$$h_0 = -\delta_p\alpha_0(\sigma_0)\ln\xi + \beta_0(\sigma_0), \tag{5.8}$$

where

$$\alpha_0 = \frac{1-\sigma_0/2}{(1-\sigma_0/2)\ln r_\infty + \tilde{\lambda}\sigma_0}, \quad \delta_p = \hat{p}_w - 1, \quad \beta_0 = 1 + \delta_p\alpha_0\ln r_\infty.$$

With such a function h_0 at hand, problem (5.4) admits a solution $\sigma_0(s,\theta)$ which does not depend on θ. To find $\sigma_0(s)$, one should solve the following Cauchy problem:

$$\frac{d\sigma_0}{ds} = \frac{\Delta_p\tilde{\lambda}(1+\sigma_0/2)}{(1-\sigma_0/2)\ln r_\infty + \tilde{\lambda}\sigma_0}, \quad \sigma_0|_{s=0} = 0, \quad \Delta_p = \frac{\delta_p}{a} \equiv \frac{A\tau(p_w - p_\infty)}{R_0^2}. \tag{5.9}$$

Now, it follows from (5.8) that h_0 does not depend on θ.

Problem (5.6)–(5.7) admits a solution

$$h_1 = H(s,\xi)\sin\theta, \quad \sigma_1 = v(s)\delta_p^{-1}\sin\theta,$$

where the functions H and v satisfy the system

$$\xi\partial_\xi(\xi\partial_\xi H) = H, \quad 1 < \xi < r_\infty, \quad H|_{\xi=r_\infty} = 0, \tag{5.10}$$

$$\xi = 1: \quad \tilde{\lambda}\left(\sigma_0\partial_\xi H + \frac{v}{\delta_p}\partial_\xi h_0\right) = (\hat{p}_w - h_0)\frac{v}{2\delta_p} + (1-\sigma_0/2)H - (1-3\sigma_0/2), \tag{5.11}$$

$$\xi = 1: \quad a\sigma_0(1-\sigma_0)^2\delta_p^{-1}\frac{dv}{ds} + a\frac{d\sigma_0}{ds}\delta_p^{-1}v(1-\sigma_0)(1-3\sigma_0)$$
$$= (1-\sigma_0)^2(1-\sigma_0/2) - 2\delta_p^{-1}v(\hat{p}_w - h_0)(1+\sigma_0/2)(1-\sigma_0)$$
$$+(1-\sigma_0)^2\left(\delta_p^{-1}v(\hat{p}_w - h_0)/2 - (1+\sigma_0/2)H\right), \quad v|_{s=0} = 0. \tag{5.12}$$

It follows from (5.10)–(5.11) that

$$H = -\alpha_1(\sigma_0, v)\xi + \beta_1(\sigma_0, v)/\xi,$$

with

$$\alpha_1 = \frac{1 - 3\sigma_0/2 - v(\tilde{\lambda}\alpha_0 + (1-\alpha_0\ln r_\infty)/2)}{\tilde{\lambda}\sigma_0(r_\infty^2+1) + (1-\sigma_0/2)(r_\infty^2-1)}, \quad \beta_1 = \alpha_1 r_\infty^2.$$

To find v, one should put $H(s,1)$ into (5.12). As a result, one obtains the following linear

https://doi.org/10.1017/S0956792507007279 Published online by Cambridge University Press

ordinary differential equation for $v(s)$:

$$\Delta_p^{-1}\frac{dv}{ds} + \alpha_2(\sigma_0)v = \beta_2(\sigma_0), \quad v|_{s=0} = 0, \tag{5.13}$$

where

$$\alpha_2 = \frac{\tilde{\lambda}(r_\infty^2(\tilde{\lambda}-1)+1+\tilde{\lambda})}{((1-\sigma_0/2)\ln r_\infty + \tilde{\lambda}\sigma_0)(\tilde{\lambda}\sigma_0(r_\infty^2+1)+(1-\sigma_0/2)(r_\infty^2-1))}$$

and

$$\beta_2 = \frac{\tilde{\lambda}(r_\infty^2+1)(1-\sigma_0/2)}{\tilde{\lambda}\sigma_0(r_\infty^2+1)+(1-\sigma_0/2)(r_\infty^2-1)}.$$

One can use two principal terms of the series (5.1) for σ to analyse the mud cake growth. We have

$$\hat{\sigma}(s,\theta) = \sigma_0(s) + \delta\delta_p^{-1}v(s)\sin\theta + o(\delta).$$

Hence, the mud cake is non-axisymmetrical provided $\delta \neq 0$. The time dependent coefficients σ_0 and v can be calculated easily using (5.9) and (5.13).

The mud cake face equation

$$\xi = 1 - \sigma_0(s) - \delta\delta_p^{-1}v(s)\sin\theta$$

in the dimensionless variables $y_i = x_i/R_0$ becomes

$$\left(y_1^2+y_2^2\right)^2 + 2\delta\delta_p^{-1}vy_2\left(y_1^2+y_2^2\right) + \delta^2\delta_p^{-2}v^2y_2^2 = (1-\sigma_0)^2\left(y_1^2+y_2^2\right).$$

Neglecting the term $\delta^2\delta_p^{-2}v^2y_2^2$, one obtains the circle

$$y_1^2 + \left(y_2 + \delta\delta_p^{-1}v\right)^2 = (1-\sigma_0(s))^2 + \delta^2\delta_p^{-2}v^2(s) \equiv d^2(s).$$

As time grows, the radius $d(s)$ of the circle decreases with the centre point $(0, -\delta\delta_p^{-1}v)$ going down when $\delta > 0$ and rising up when $\delta < 0$.

In what follows, we use two principal terms of the series (5.1) for $\hat{h}$ to analyse the invasion front.

6 Invasion front equations

Since the density of the formation fluid is constant and coincides with that of the invading fluid, the salt distribution in the formation is described by the following equations [2]:

$$\Phi_r\frac{\partial c}{\partial t} + \operatorname{div}(c\,\mathbf{q}) = 0, \quad \operatorname{div}\mathbf{q} = 0, \quad \mathbf{q} = -\lambda_r\nabla h, \quad h \equiv p + \rho_f^r g x_2. \tag{6.1}$$

The following notations are adopted: c is the salt mass concentration and Φ_r is the reservoir porosity. The rock reservoir mobility λ_r does not depend on c and hence the salt transport equation in (6.1) is uncoupled from the last two equations. The only role of the first equation in (6.1) is to work out the interface between the original pore fluid and the invading filtrate. Having the same density and the same viscosity, these two fluids are distinguished by the salt concentration only.

https://doi.org/10.1017/S0956792507007279 Published online by Cambridge University Press

The salt boundary and initial conditions are:

$$c|_{r=R_0} = c_1, \quad c|_{t=0} = c_0. \tag{6.2}$$

Hence, the salt concentration c in the invasion domain and in the virgin rock formation takes the values c_1 and c_0 respectively. We note that the first of conditions (6.2) for c is meaningful only for those points of the circle $r = R_0$ at which the seepage velocity $\mathbf{q}$ is directed into the formation, i.e. the following inequality should be satisfied:

$$r = R_0 : \quad \partial_r h \leqslant 0. \tag{6.3}$$

Let us return to the dimensionless variables. Neglecting terms of order $o(\delta)$, we have the following representation formula for the reservoir potential $\hat{h}$:

$$\hat{h} = \beta_0(s) - \delta_p \alpha_0(s) \ln \xi + \delta(-\alpha_1(s)\xi + \beta_1(s)/\xi) \sin\theta. \tag{6.4}$$

This representation implies that the flow pattern is symmetric with respect to the vertical axis. In terms of the dimensionless variables $y_i = x_i/R_0$, we find the stream function ψ from the conditions $\psi_{y_1} = \hat{h}_{y_2}$, $\psi_{y_2} = -\hat{h}_{y_1}$ using the curvilinear integral

$$\psi(y_1, y_2) = \int_{(y_1^0, y_2^0)}^{(y_1, y_2)} -\hat{h}_{y_1} dy_2 + \hat{h}_{y_2} dy_1 = \int_{L_1} \cdots + \int_{L_2} \cdots .$$

Here,

$$(y_1, y_2) = (\xi\cos\theta, \xi\sin\theta), \quad (y_1^0, y_2^0) = (1, 0).$$

The segment L_1 connects the point (y_1^0, y_2^0) with the point $(y_1^*, y_2^*) = (\xi, 0)$. The segment L_1 is defined in the parametric form

$$L_1 : \quad y_1 = 1 + \zeta(\xi - 1), \quad y_2 = 0, \quad 0 \leqslant \zeta \leqslant 1.$$

The curvilinear segment L_2 is a part of the circumference defined in the parametric form

$$L_2 : \quad y_1 = \xi\cos(\zeta\theta), \quad y_2 = \xi\sin(\zeta\theta), \quad \tan\theta = y_1/y_2, \quad 0 \leqslant \zeta \leqslant 1.$$

Each integral $\int_{L_i}$ is evaluated parametrically to give the following representation for the dimensionless stream function ψ in the polar coordinates:

$$\psi(\xi, \theta) = \delta_p \alpha_0 \theta - \delta(\alpha_1 \xi + \beta_1/\xi)\cos\theta + \text{const}.$$

Now, the trajectory of each fluid particle that issues from the point of the wellbore $(1, \theta_0)$ is specified by the equality $\psi(\xi, \theta) = \psi(1, \theta_0)$.

The salt transport equation in the dimensionless polar variables becomes

$$\partial_s \hat{c} - \Lambda(\partial_\xi \hat{c}\, \partial_\xi \hat{h} + \xi^{-2} \partial_\theta \hat{c}\, \partial_\theta \hat{h}) = 0, \quad \Lambda = \frac{\lambda_r p_\infty \tau}{R_0^2 \Phi_r},$$

https://doi.org/10.1017/S0956792507007279 Published online by Cambridge University Press

or

$$\partial_s \hat{c} + \Lambda \left(\delta_p \alpha_0 \xi^{-1} + \delta\left(\alpha_1 + \beta_1 \xi^{-2}\right) \sin\theta\right) \partial_\xi \hat{c} - \delta \Lambda \cos\theta\left(-\alpha_1 \xi^{-1} + \beta_1 \xi^{-3}\right) \partial_\theta \hat{c} = 0.$$

The characteristics of this equation are specified by

$$\begin{aligned} \frac{d\xi}{ds} &= \Lambda_1 \alpha_0(\sigma_0)\xi^{-1} + \Lambda_2(\alpha_1(\sigma_0, v) + \beta_1(\sigma_0, v)\xi^{-2}) \sin\theta, \quad \xi(0) = 1, \\ \frac{d\theta}{ds} &= \Lambda_2(\alpha_1(\sigma_0, v)\xi^{-1} - \beta_1(\sigma_0, v)\xi^{-3}) \cos\theta, \quad \theta(0) = \theta_0 \in \left[-\frac{\pi}{2}, \frac{\pi}{2}\right], \end{aligned} \tag{6.5}$$

where

$$\Lambda_1 = \delta_p \Lambda = \frac{\lambda_r \tau (p_w - p_\infty)}{R_0^2 \Phi_r}, \quad \Lambda_2 = \delta \Lambda = \frac{\lambda_r \tau g \left(\rho_f^r - \rho_m\right)}{R_0 \Phi_r}.$$

To construct the invasion front, it suffices to find a solution of system (6.5):

$$\xi = \xi(s, \theta_0), \quad \theta = \theta(s, \theta_0), \quad \theta_0 \in \left[-\frac{\pi}{2}, \frac{\pi}{2}\right]. \tag{6.6}$$

Equations (6.6) define a parametric specification of this front, with θ_0 being a parameter. Elimination of θ_0 results in the front equation

$$\xi = \xi(s, \theta). \tag{6.7}$$

We denote

$$v = \sin\theta, \quad B_1 = \Lambda_2 \alpha_1(\sigma_0, v), \quad B_2 = \Lambda_2 \beta_1(\sigma_0, v), \quad B_3 = \Lambda_1 \alpha_0(\sigma_0),$$

then problem (6.6) becomes equivalent to

$$\begin{aligned} \frac{d\xi}{ds} &= B_3 \xi^{-1} + \left(B_1 + B_2 \xi^{-2}\right) v, \quad \xi(0) = 1, \\ \frac{dv}{ds} &= (1 - v^2)\left(B_1 \xi^{-1} - B_2 \xi^{-3}\right), \quad v(0) = v_0 \in [-1, 1]. \end{aligned} \tag{6.8}$$

We remark that the three-dimensional invasion cone along a horizontal wellbore can be calculated by system (6.8) as far as the drilling velocity is known [3].

The behavior of the front is strongly determined by the parameters δ_p and δ. Depending on the sign of δ, three cases are possible: $\delta = 0$, $\delta > 0$ and $\delta < 0$. We consider them sequentially.

7 Axisymmetrical invasion

Let $\rho_f^r = \rho_m$. Due to (6.4), the necessary invasion condition (6.3) in the case $\delta = 0$ becomes

$$\max_\theta \partial_\xi \hat{h}|_{\xi=1} \equiv -\delta_p \alpha_0 \leqslant 0.$$

Clearly it is valid if $\delta_p \geqslant 0$. The mud cake is an annulus domain, with the dimensionless thickness equal to σ_0 and growing according to the law (5.9). When $B_1 = B_2 = 0$, the

https://doi.org/10.1017/S0956792507007279 Published online by Cambridge University Press

front is defined by the equations

$$\frac{d\xi}{ds} = \frac{B_3(\sigma_0)}{\xi}, \quad \frac{dv}{ds} = 0, \quad \xi(0) = 1, \quad v(0) = v_0 \in [-1, 1]. \tag{7.1}$$

It follows from (5.9) and (7.1) that

$$\frac{d\xi^2}{d\sigma_0} = \frac{2a\Lambda(1 - \sigma_0/2)}{\tilde{\lambda}(1 + \sigma_0/2)}.$$

Hence, the front is a circumference with centre at the coordinate origin and radius specified by the formula

$$\xi^2 = 1 + \gamma(\ln(1 + \sigma_0/2) - \sigma_0/4), \quad \gamma = 8a\Lambda/\tilde{\lambda}. \tag{7.2}$$

Particularly, this law enables one to evaluate the invasion zone by means of the mud cake thickness growth given by Caliper measurements. (Observe, that the right-hand side of (7.2) is an increasing function of σ_0.) The law (7.2) helps also to determine the relative velocity factor α introduced by (3.7). Indeed, let the invasion front radius $\xi = r_\star$ correlate statistically with the mud cake thickness $\sigma_0 = \sigma_0^\star$, as far as the vertical wellbore is concerned. Then one can calculate the constant a and eventually the constant α by the formula

$$\frac{r_\star^2 - 1}{\ln(1 + \sigma_0^\star/2) - \sigma_0^\star/4} = \gamma,$$

and formulas (3.10) and (4.5).

There is one more conclusion from (7.2). Let $\xi = r_\star$ and $\sigma_0 = \sigma_0^\star$ be laboratory measurement data (obtained at the same instant); then the *in situ* data $(\xi(s), \sigma_0(s))$ should obey the formula

$$\frac{\xi^2(s) - 1}{\ln(1 + \sigma_0(s)/2) - \sigma_0(s)/4} = \frac{r_\star^2 - 1}{\ln(1 + \sigma_0^\star/2) - \sigma_0^\star/4}, \tag{7.3}$$

provided the laboratory and *in situ* conditions are characterized by the same dimensionless parameter γ.

8 Non-axisymmetrical invasion

Assume $\delta \neq 0$. There is a time interval $(0, s_*)$, such that both $\alpha_1(s)$ and $\beta_1(s)$ are strictly positive when $0 < s < s_*$. Due to (6.4), the invasion condition (6.3) becomes

$$\max_\theta \partial_\xi \hat{h}|_{\xi=1} \equiv |\delta|(\alpha_1(s) + \beta_1(s)) - \delta_p \alpha_0(s) \leqslant 0, \quad 0 < s < s_*.$$

Particularly, this inequality is valid if the parameters δ_p and δ obey the restriction

$$\frac{\delta_p}{|\delta|} \equiv \frac{p_w - p_\infty}{gR_0|\rho_f^r - \rho_m|} \geqslant D, \tag{8.1}$$

https://doi.org/10.1017/S0956792507007279 Published online by Cambridge University Press

where

$$D \equiv \sup_{0\leqslant\sigma\leqslant 2/3} \frac{(1+r_\infty^2)(1-3\sigma/2)(\tilde{\lambda}\sigma+(1-\sigma/2)\ln r_\infty)}{(1-\sigma/2)(\tilde{\lambda}\sigma(1+r_\infty^2)+(1-\sigma/2)(r_\infty^2-1))}.$$

Clearly, $D \geqslant D_* \equiv ((1+r_\infty^2)\ln r_\infty)/(r_\infty^2-1)$. Below, some simulations will be performed at the minimal pressure overbalance condition with

$$p_w = p_{w,min} \equiv p_\infty(1+D_*|\delta|). \tag{8.2}$$

Observe, that low pressure overbalance is widely applied in the drilling practice to minimize the formation damage.

Let the inequality (8.1) hold with $\delta > 0$. We analyse the invasion front using the following mathematical claim. The function $\xi(s,\theta)$ in (6.7), which specifies the front, increases monotonically with increase in θ for $\theta \in [-\pi/2, \pi/2]$. In this case

$$\partial_\theta \xi > 0 \quad \text{if} \quad -\frac{\pi}{2} < \theta < \frac{\pi}{2} \quad \text{and} \quad \partial_\theta \xi = 0 \quad \text{if} \quad \theta = \pm\frac{\pi}{2}. \tag{8.3}$$

Let us prove this statement locally in time. Since $\partial_\theta \xi = \partial_v \xi \cos\theta$, it suffices to establish that

$$\partial_v \xi(s,v) > 0 \quad \text{for} \quad 0 < s < s_0, \quad -1 \leqslant v \leqslant 1, \tag{8.4}$$

where $(0, s_0)$ is a time interval and

$$\xi = \xi(s,v), \tag{8.5}$$

is the equation of the boundary of the invasion front in the dimensionless variables v and ξ for fixed $s > 0$.

Let us differentiate equality (8.5) with respect to v_0:

$$\frac{d\xi}{dv_0} = \frac{d\xi}{dv}\frac{dv}{dv_0}, \quad \frac{d\xi}{dv} = \frac{\chi}{\omega}, \quad \chi \equiv \frac{d\xi}{dv_0}, \quad \omega \equiv \frac{dv}{dv_0}.$$

The functions $\chi(s,v_0)$ and $\omega(s,v_0)$ obey the initial conditions

$$\chi(0,v_0) = 0, \quad \omega(0,v_0) = 1, \tag{8.6}$$

and satisfy the equations:

$$\begin{aligned} \frac{d\chi}{ds} &= -B_3\xi^{-2}\chi - 2B_2\xi^{-3}v\chi + \big(B_1 + B_2\xi^{-2}\big)\omega, \\ \frac{d\omega}{ds} &= (1-v^2)\big(-B_1\xi^{-2} + 3B_2\xi^{-4}\big)\chi - 2\big(B_1\xi^{-1} - B_2\xi^{-3}\big)v\omega, \end{aligned} \tag{8.7}$$

which are obtained by differentiation of (6.8) with respect to v_0. Considering the first equation of system (8.8) as an ordinary differential equation for χ, we obtain the following

https://doi.org/10.1017/S0956792507007279 Published online by Cambridge University Press

representation:

$$\chi(s,v_0)=A_1\int_0^s\omega(t,v_0)G_1(t,v_0)dt,\quad A_1(s,v_0)=\exp\left(\int_0^s F_1(t,v_0)dt\right),$$
$$F_1(s,v_0)=-\frac{B_3}{\xi^2}-\frac{2vB_2}{\xi^3},\quad G_1(s,v_0)=\left(B_1+\frac{B_2}{\xi^2}\right)A_1^{-1}(s,v_0). \tag{8.8}$$

Due to the initial conditions (8.6) for ω, there is a time interval $[0,s_1]$ such that $\omega(s,v_0)$ is strictly positive uniformly in $v_0\in[-1,1]$. On the other hand, there is a time interval $[0,s_2]$ such that $B_1(s)\geqslant 0$ and $B_2(s)\geqslant 0$ for $0<s<s_2$. It follows from (8.8) that $\chi>0$ for all $0<s<s_3$, $s_3=\min\{s_1,s_2\}$, uniformly in $v_0\in[-1,1]$. Therefore, $\chi/\omega>0$ for $0<s<s_3$ uniformly in $v_0\in[-1,1]$. Thus, inequality (8.4) and relations (8.3) are verified.

In the case $\delta<0$, the front geometry is analysed performed by the same scheme as for $\delta>0$. For this, it suffices to replace the positive functions B_1 and B_2 by the negative ones: $B_1:=-|B_1|$, $B_2:=-|B_2|$. We give only the final results. At each fixed time, the monotonicity property of the front is expressed by the conditions

$$\partial_\theta\xi<0\quad\text{if}\quad-\frac{\pi}{2}<\theta<\frac{\pi}{2}\quad\text{and}\quad\partial_\theta\xi=0\quad\text{if}\quad\theta=\pm\frac{\pi}{2}. \tag{8.9}$$

Interestingly, the front is a symmetric reflection (relative to the horizontal axis $x_2=0$) of the front obtained for the case $\delta>0$. This is a consequence of the fact that system (6.5) has the following symmetry. Let $\delta<0$. We denote the solution of problem (6.5) by $(\xi(s;\delta,\theta_0),\theta(s;\delta,\theta_0))$ and introduce the functions $\xi_*(s)=\xi(s;\delta,\theta_0)$ and $\theta_*(s)=-\theta(s;\delta,\theta_0)$. Then, it is easy to verify that (ξ_*,θ_*) is a solution of problem (6.5) if δ is replaced by $|\delta|$ and θ_0 by $-\theta_0$, i.e.

$$\frac{d\xi_*}{ds}=B_3\xi_*^{-1}+(|B_1|+|B_2|\xi_*^{-2})\sin\theta_*,\quad\xi_*(0)=1,$$
$$\frac{d\theta_*}{ds}=(|B_1|\xi_*^{-1}-|B_2|\xi_*^{-3})\cos\theta_*,\quad\theta_*(0)=-\theta_0\in\left[-\frac{\pi}{2},\frac{\pi}{2}\right].$$

9 Loss of convexity

Let us consider the case $\delta<0$. Clearly, system (6.8) has two solutions $(\xi=\xi_1(s),v=-1)$ and $(\xi=\xi_2(s),v=1)$, where

$$\frac{d\xi_1}{ds}=\frac{B_3}{\xi_1}-\frac{B_2}{\xi_1^2}-B_1,\quad\frac{d\xi_2}{ds}=\frac{B_3}{\xi_2}+\frac{B_2}{\xi_2^2}+B_1,\quad\xi_1(0)=\xi_2(0)=1. \tag{9.1}$$

Hence, the distances $\xi_1(s)$ and $\xi_2(s)$ are the largest and smallest offset front distances from the centre at the moment s. In what follows, we will show numerically that the invasion front can lose convexity with time at the closest front's point $P_2=(x_1,x_2)=(0,\xi_2(s))$. Observe that the front maintains its convexity for some time because of continuous dependence upon initial data. The calculation scheme is formed as follows. Given an instant s, we compare the line tangent to the front point P_2 and the horizontal line $x_2=\xi_2(s)$. The latter is specified in the polar coordinates (ξ,v), $v=\sin\theta$, by the equation

https://doi.org/10.1017/S0956792507007279 Published online by Cambridge University Press

$\xi = \xi_2(s)v^{-1}$. For such a line, $d\xi/dv = -\xi_2(s)v^{-2}$. Therefore, for the front equation $\xi = \xi(v,s)$, it suffices to establish that the inequality

$$J(s) := \frac{d\xi}{dv}|_{v=1} < -\xi_2(s), \tag{9.2}$$

holds starting from a certain moment. Setting $v = 1$ in formulas (6.8), we find that the function $J(s) := \chi/\omega|_{v=1}$, with χ and ω defined in Section 8, satisfies the equation

$$\frac{dJ}{ds} = -\left(\frac{4B_2}{\xi_2^3} + \frac{2B_1}{\xi_2} + \frac{B_3}{\xi_2^2}\right) J + B_1 + \frac{B_2}{\xi_2^2}, \quad J(0) = 0. \tag{9.3}$$

One can solve numerically equation (9.3) jointly with (5.9), (5.13) and equation (9.1) for r_2 to show that inequality (9.2) may be valid starting from a certain moment with a special choice of data (for example, δ_p should be sufficiently small).

If $\delta > 0$, the convexity loss occurs by symmetry at the nearest front point where $\theta = -\pi/2$. Observe, that in [11], the loss of convexity was proved analytically for the invasion model with a stable mud cake.

10 Numerical results

The data below are taken from [3] for the water based mud. Making use of Mathematica 5, we perform a series of calculations varying some data. First, we list the invariable data: $R_0 = 10\,cm$, $r_\infty = 40$, $\rho_f^r = 0.84\,g/cm^3$, $\rho_c = 3.0\,g/cm^3$, $\rho_f^- = 1.0\,g/cm^3$, $\rho_f^+ = 1.00001\,g/cm^3$, $\rho_s^- = 2.4\,g/cm^3$, $\rho_s^+ = 3.0\,g/cm^3$, $\varphi_s^- = 2.65\%$, $\varphi_s^- + \varphi_f^- = 1$, $\Phi_c = 20\%$, $\varphi_s^+ = 1 - \Phi_c$, $\rho_m \equiv \varphi_s^-\rho_s^- + \varphi_f^-\rho_f^- = 1.037\,g/cm^3$, $\Phi_r = 36\%$, $\mu_c = 0.6\,cp = 0.006\,g/(cm\cdot s)$, $\mu_r = 3\,cp = 0.03\,g/(cm\cdot s)$, $\tau = 3600\,s$, $r_* = 10$.

In the simulations below, we calculate the farthest front point with the coordinates $(0, -R_0\xi_1(s))$, the front point $(0, R_0\xi_2(s))$ which is nearest the wellbore centre, the loss of axisymmetry $R_0\xi_1(s) - R_0\xi_2(s)$ and the mean value of the mud cake thickness $R_0\sigma_0(s)$. Their is no a loss of convexity in the first two simulations. Let us denote $r_i = R_0\xi_i$ and $\sigma = R_0\sigma_0$.

Simulation 1. Here $k_r = 100\,md = 0.987\times 10^{-9}\,cm^2$, $k_r/k_c = 100$, $p_\infty = 100\,bar = 10^6\,g/(cm\cdot s)$, $p_w = 120\,bar$, $\sigma_0^* = 0.03$. The following results are obtained at $s = 16$ hours: $\delta = -0.193158\times 10^{-4}$, $r_1 = 175\,cm$, $r_1 - r_2 = 3\times 10^{-4}\,cm$, $\sigma = 3.0\,cm$. Clearly, both the mud cake and the invasion zone can be considered annuli (Figure 2).

Simulation 2. Here $k_r = 100\,md$, $k_r/k_c = 100$, $p_\infty = 100\,bar$, $p_w = p_{w,min} = 100.007\,bar$, $\sigma_0^* = 0.03$. The following results are obtained at $s = 16$ hours: $\delta = -0.193158\times 10^{-4}$, $r_1 = 11.75\,cm$, $r_1 - r_2 = 1.75\,cm$, $\sigma = 0.00008\,cm$. The front non-axisymmetry is strong (Figure 3).

A loss of convexity is observed in the next five simulations. *Simulation 3.* Here $k_r = 100\,md$, $k_r/k_c = 100$, $p_\infty = 1\,bar$, $p_w = p_{w,min} = 1.007\,bar$, $\sigma_0^* = 0.03$. The following results are obtained at $s = 800$ hours: $\delta = -0.193158\times 10^{-2}$, $r_1 = 35\,cm$, $r_1 - r_2 = 16.5\,cm$, $\sigma = 0.04\,cm$. A loss of convexity occurs soon after $s = 400$ hours (Figure 4).

Next four simulations are characterized by the same value of $\delta = -0.193158\times 10^{-2}$. Their common features are $\sigma_0^* = 0.1$ and the minimal pressure overbalance conditions (8.2), i.e. $p_\infty = 1\,bar$, $p_w = 1.00713\,bar$. We vary only values of k_r and k_c.

https://doi.org/10.1017/S0956792507007279 Published online by Cambridge University Press

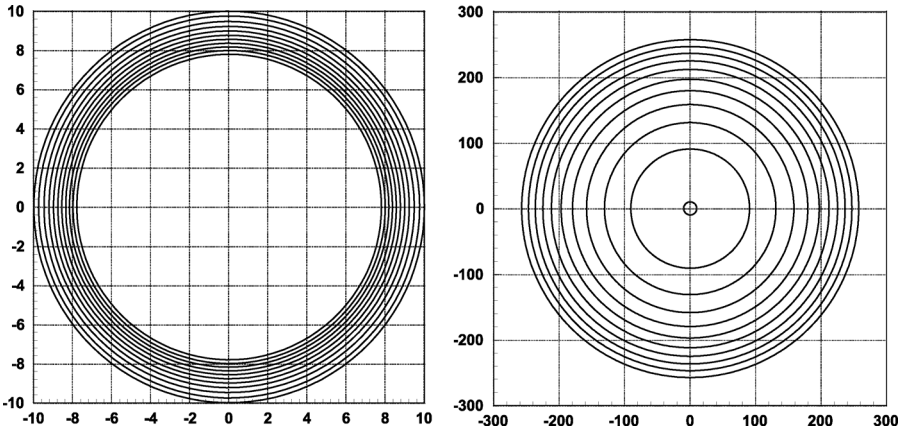

FIGURE 2. Mud cake face and invasion front calculated in Simulation 1 for s = 30 h.

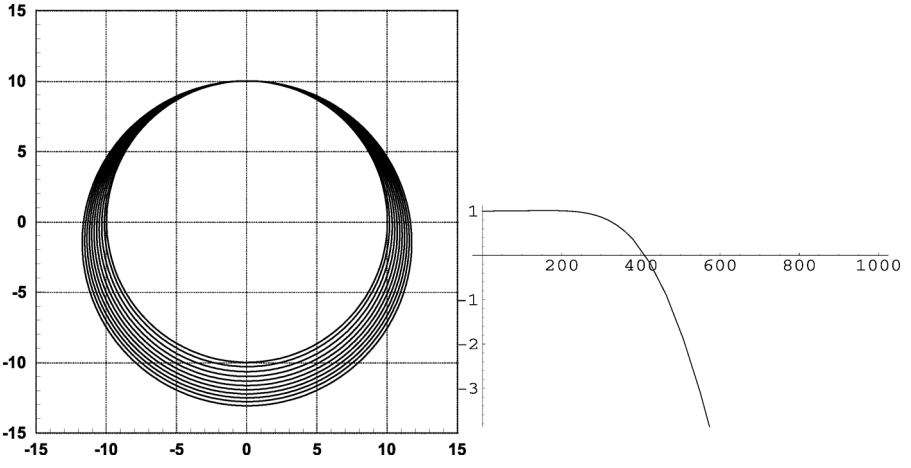

FIGURE 3. Invasion front in Simulation 2 at s = 30 h. Plot of $J + \xi_2$.

Simulation 4 with the data $k_r = 10000\,md$ and $k_r/k_c = 10$ hours. The following results are obtained at $s = 10$: $r_1 = 40\,cm$, $r_1 - r_2 = 22\,cm$, $\sigma = 0.175\,cm$. An invasion front non-axisymmetry is clearly developed and a loss of convexity is observed for $s > 3.75$ hours.

Simulation 5 with the data $k_r = 1000\,md$ and $k_r/k_c = 10$. The following results are obtained at $s = 100$ hours: $r_1 = 40\,cm$, $r_1 - r_2 = 20\,cm$, $\sigma = 0.175\,cm$. An invasion front non-axisymmetry is clearly developed and a loss of convexity is observed for $s > 37$ hours.

Simulation 6 with the data $k_r = 100\,md$ and $k_r/k_c = 10$. The results are obtained at $s = 800$ hours: $r_1 = 40\,cm$, $r_1 - r_2 = 18\,cm$, $\sigma = 0.14\,cm$. An invasion front non-axisymmetry is clearly developed and a loss of convexity is observed for $s > 375$ hours.

Simulation 7 with the data $k_r = 100\,md$ and $k_r/k_c = 1$. The results are obtained at $s = 1000$ hours: $r_1 = 45\,cm$, $r_1 - r_2 = 20\,cm$, $\sigma = 0.175\,cm$. An invasion front non-axisymmetry is clearly developed and a loss of convexity is observed for $s > 350$ hours.

https://doi.org/10.1017/S0956792507007279 Published online by Cambridge University Press

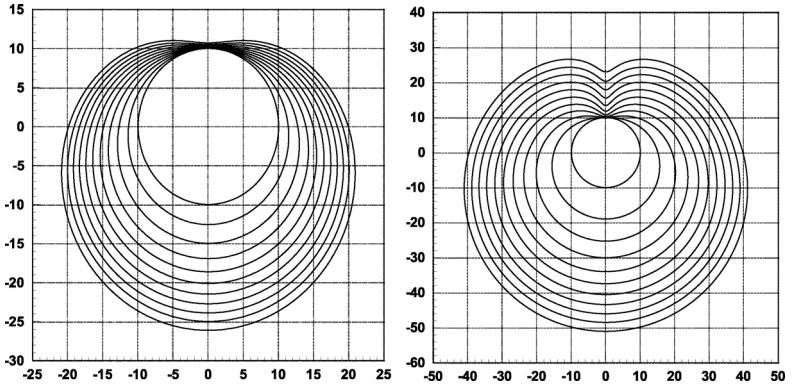

FIGURE 4. Invasion front in Simulation 3 at $s > 400$ h. Invasion front in Simulation 7 at $s = 1500$ h.

Conclusions

The goal of the study is to estimate the role of gravitation as far as the drilling mud-filtrate invasion around a horizontal wellbore is concerned. A mathematical model is formulated to simulate both the invasion and mud cake development under application of overbalanced pressure. Real drillings with the water based mud are characterised by small values of the dimensionless gravitational parameter $|\delta| = gR_0(\rho_m - \rho_f^r)/p_\infty (\approx 10^{-2} - 10^{-5})$. Under the assumption that the mud cake is thin, an asymptotic theory is developed to reduce the model to four ordinary differential equations. As the theory reveals, there are five principal dimensionless parameters

$$\frac{\lambda_r}{\lambda_c}, \quad \frac{R_\infty}{R_0}, \quad \frac{\lambda_r \tau (p_w - p_\infty)}{R_0^2 \Phi_r}, \quad \frac{\lambda_r \tau g \left(\rho_f^r - \rho_m\right)}{R_0 \Phi_r}, \quad \frac{\tau (p_w - p_\infty) \alpha \rho_s^- \rho_f^r \varphi_s^- \lambda_c}{\rho_f^w \varphi_f^- (\rho_c (1 - \Phi_c) - \rho_s^- \varphi_s^-)}$$

which characterise the evolution both of the invasion front and of the mud cake. This implies that a laboratory experiment is meaningful and simulate an *in situ* experiment provided the laboratory input principal parameters and the *in situ* principal parameters coincide.

We have proved by analytical tools that non-axisymmetry both of invasion front and of mud cake always occurs if a water based drilling mud is applied. The invasion region annulus is the most thicker below and the most thinner above. The same is true for the mud cake annulus.

Numerical calculations have demonstrated that the non-axisymmetry degree strongly depends on the pressure overbalance parameter $\Delta_p = (p_w - p_\infty)/(gR_0|\rho_f^r - \rho_m|)$. For high values of Δ_p, both the mud cake and the damage zone can be assumed regular annuli. Invasion profile non-axisymmetry manifests itself for low values of Δ_p. One more feature of simulations with low values of Δ_p is a loss of the front convexity.

The impact of different parameters on the invasion profile has been studied. Among the most influential are formation permeability and mud cake permeability as well. This is why accurate laboratory measurements of mud cake permeability are necessary. Being simple, the model should be improved by taking into account mud circulation and by integrating more general reservoir properties.

https://doi.org/10.1017/S0956792507007279 Published online by Cambridge University Press

Acknowledgements

The research was partially supported by Russian Fund of Fundamental Researches (grant 05-01-00131) and the Programme 14.4.2 of Russian Academy of Sciences. Numerical simulations were performed with the support of Baker Hughes, Novosibirsk. The author would like to thank Andrey Eremchenko for his assistance with computations.

References

[1] Alpak, F. O., Dussan, E. B., Habashy, T. & Torres-Verdin, C. (2002) Numerical simulation of mud-filtrate invasion in horizontal wells and sensitivity analysis of array induction tools. *SPWLA Ann. Log. Symp. June (2–5)*, 43.

[2] Chavent, G. & Jaffre, J. (1986) *Mathematical models and finite elements for reservoir simulation.* North-Holland, Amsterdam, 34.

[3] Ding, Y., Longeron, D., Renard, G. & Audibert, A. (2004) Modelling of both near-wellbore damage and natural cleanup of horizontal wells drilled with water-based drilling fluids. *SPE Journal* 9(3), 252–264.

[4] Fisher, K. A., Wakeman, R. J., Chiu, T. W. & Meuric, O. F. J. (2002) Numerical modelling of cake formation and fluid loss from non-newtonian muds during drilling using eccentric/concentric drill strings with/without rotation. *Trans. IChemE* 78(A), 707.

[5] Godlevski, E. & Raviart, P. A. (1991) *Hyperbolic Systems of Conservation Laws. Mathematiques et Applications.* SMAI. Ellipses, Paris, 34.

[6] Ishii, M. (1975) *Thermo-fluid Dynamic Theory of Two-phase Flow*. Eyrolles, Paris.

[7] Johnson, R. S. (1997) *A Modern Introduction to the Mathematical Theory of Water Waves.* Cambridge University Press, Cambridge.

[8] Lu, W. M. & Ju, S. C. (1989) Selective particle deposition on crossflow filtration. *Separ. Sci. and Technol.* 24(7–8), 517.

[9] Moiseev, N.N. (1981) *Asymptotic Methods of Nonlinear Mechanics.* Science, Moscow. (in Russian).

[10] Peeters, M., Kovats, J., & Moita, C., et al. (2002) Monitoring and modeling invasion using ground penetrating radar and flow simulation programs. *SPWLA Ann. Log. Symp. June (2–5)*, 43.

[11] Shelukhin, V. V. & Yeltsov, I. N. (2004) Invasion zones in lateral drilling. *J. Appl. Mech. Tech. Phys.* 45(6), 834–842.

[12] Smaller, J. (1983) *Shock Waves and Reaction-diffusion Equations.* Berlin-Heidelberg-New York. Springer-Verlag.

[13] Stamatakis, K. & Tien, C. (1993) A simple model of crossflow filtration based on particle adhesion. *AIChEJ* 39(8), 1292.

[14] Thomas, B. & Sharma, M. M. (1997) Distribution of mud induced damage around horizontal wellbore. *SPE International Simposium on Formation Damage Control, SPE 39468. Lafayette, Louisiana, February 18–19.*